Mathematical Biosciences and Engineering

MBE, 20(2): 2651–2668.
DOI: 10.3934/mbe.2023124
Received: 25 September 2022
Revised: 06 November 2022
Accepted: 07 November 2022
Published: 25 November 2022

http://www.aimspress.com/journal/MBE

Research article

Numerical simulation and experimental study for ultrasonic vibration-assisted drilling of SiCp/AL6063

Xu Ji[1], Fan Bai[1], Jiang Jiang[2], Hongge Fu[1,*], Qingjie Sun[1] and Weiyu Zhu[1]

[1] School of Mechanical and Electrical Engineering, North China Institute of Aerospace Engineering, 133 Aimin East Road, Langfang, Hebei, China
[2] Department of Additive Manufacturing, Beijing Spacecrafts Manufacturing Factory, 104 Youyi road, Haidian District, Beijing, China

* **Correspondence:** Email: fhg800922@nciae.edu.cn; Tel: +8615611663609.

Abstract: Thrust force and metal chips are essential focuses in SiCp/AL6063 drilling operations. Compared with conventional drilling (CD), the ultrasonic vibration-assisted drilling (UVAD) has attractive advantages: for instance, short chips, small cutting forces, etc. However, the mechanism of UVAD is still inadequate, especially in the thrust force prediction model and numerical simulation. In this study, a mathematical prediction model considering the ultrasonic vibration of the drill is established to calculate the thrust force of UVAD. A 3D finite element model (FEM) for the thrust force and chip morphology analysis is subsequently researched based on ABAQUS software. Finally, experiments of CD and UVAD of SiCp/Al6063 are performed. The results show that when the feed rate reaches 151.6 mm/min, the thrust force of UVAD decreases to 66.1 N, and width of the chip decreases to 228 um. As a result, the errors of the mathematical prediction and 3D FEM model of UVAD are about 12.1 and 17.4% for the thrust force, and the errors of the CD and UVAD of SiCp/Al6063 are 3.5 and 11.4% for the chip width, respectively. Compared with the CD, UVAD could reduce the thrust force and improve chip evacuation effectively.

Keywords: UVAD; mathematical prediction model; 3D FEM; chip morphology

1. Introduction

SiCp/Al6063 is a widely used metal matrix composite material. It has excellent performance in

terms of its low weight, high hardness, good fatigue resistance, good toughness, specific modulus and high dimensional stability [1−3]. Good performance makes it used in automotive, electronic packaging, aerospace, ships, weapons, and precision equipment. Although SiCp/Al6063 has premium properties such as high strength and low ductility, there are large thrust force, poor quality of the entrance, serious tool wear and other problems. Therefore, a lot of researchers have conducted studies on the problems.

In recent years, some scholars have revealed that, when compared to conventional machining, the ultrasonic vibration-assisted machining with high-frequency and small-amplitude has exhibited good cutting performances for difficult-to-cut materials [4]. In mechanical manufacturing processes, ultrasonic vibration could reduce the machining force through intermittent cutting between machine tools and the work-piece and decrease the load in both densification and forming processes due to the reduced friction [5]. The principle of ultrasonic vibration-assisted manufacturing is shown in Figure 1. The ultrasonic vibration frequency parameter is input by the controller to control the movement of the motor on the tool handle. So, the ultrasonic vibration movement of tool is increased, which shortens the contact time between the tool and work-piece effectively. Also, it could improve the machining quality.

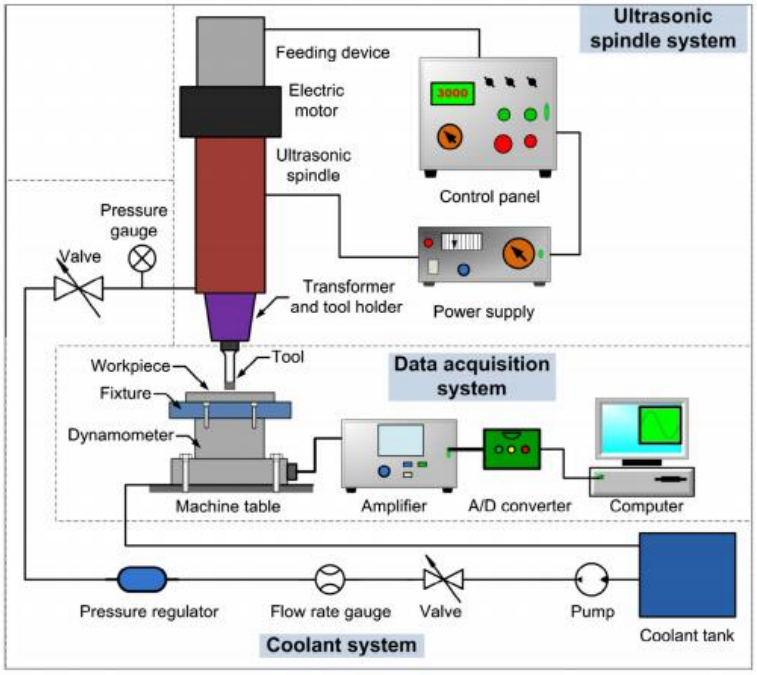

Figure 1. Device principle of UVAD [6].

Recently, many scholars have made progress in the research field of the ultrasonic vibration-assisted manufacturing of difficult-to-cut materials. Most of the ultrasonic vibration-assisted manufacturing processes focus on force and chip shape changes, etc. Zha et al. [7] carried out the ultrasonic vibration-assisted scratch experiment for SiCp/Al composite material, and the research showed that the cutting force is smaller than conventional scratch in the machining process. Wang et al. [8] compared the capacity of conventional grinding and ultrasonic vibration-assisted grinding of SiCp/Al composite material; the result indicated that ultrasonic vibration-assisted grinding can reduce the contact force and improve the machining quality. Qin et al. [9] used longitudinal torsional

ultrasonic vibration-assisted milling (LTUAM) technology to process high-strength titanium alloy Ti-6Al-4V. The result showed that, compared with CM, the cutting force of LTUAM is significantly reduced due to the high-frequency intermittent cutting mechanism caused by ultrasonic vibration. In terms of UVAD, Scholars have explored comprehensive discussion for the thrust force and chip changes. Junichiro et al. [10] pointed out that UVAD is a discontinuous processing mode, which could reduce the friction and plastic deformation in the cutting deformation zone. So, it could reduce the thrust force and temperature. Zhu et al. [11] carried out UVAD micro-hole experiments to compare with the CD, UVAD reduced thrust force. Baraheni et al. [12] found the thrust force is lower while studying the UVAD process of aviation aluminum alloy (AA7075). In addition, the comparison between UVAD and CD thrust force of aluminum alloy by Li et al. [13] showed that UVAD thrust force is smaller than CD. All these studies were in line with the conclusion proposed by Junichiro and verified the mechanism of UVAD thrust force reduction. Moreover, some scholars studied the degree of thrust force reduction using UVAD. Compared with the CD, Gao et al. [14] found that the average thrust force was reduced by 1.98 to 24.9% in ultrasonic vibration–assisted micro-hole drilling of Ti-6Al-4V. Li et al. [15] carried out a fundamental investigation into rotational UVAD on ceramic matrix composites of C/SiC, and the result showed that reduction rate of specific drilling energy of rotational UVAD decreased from over 30% to less than 15% compared with CD. Li et al. [16] found that the thrust force reduced by 26% in UVAD of Ti-6Al-4V and also with good machining. Abdelaziz et al. [17] explored the differences between UVAD and CD under different feed rates. UVAD improved the quality of hole, for instance, the hole error of cylindricity was reduced by 33%, and the thrust force and torque were reduced by 18.5% and 20% on average respectively. Furthermore, some researchers analyzed the advantages of chip removal in ultrasonic vibration-assisted manufacturing. Studies show that the bending degree and size of conventional drilling milling (CM) chips are much larger than ultrasonic vibration-assisted milling (UVAM) chips [18]. Niu et al. [19] found that the amplitude is the main factor affecting the chip shape in UVAM of 20% SiCp/Al composite. Li et al. [20] revealed that UVAD has good chip damage and chip removal effect, good drilling surface integrity in the comparative experiment study of titanium alloy. Meanwhile, Xu et al. [21] also showed that UVAD could improve discharge chips. According to the research, UVAD of difficult-to-cut materials has advantages of significantly decreasing thrust force, improving discharge chips.

Considering the processing advantages of UVAD, some scholars have carried out corresponding research on prediction model. As a result, the UVAD prediction model can be divided into 3D FEM and mathematical thrust force prediction model. For 3D FEM of SiCp/Al6063 composite materials, a small amount of work has been carried out. Dou et al. [22] proposed a new constitutive model, established a 3D FEM and verified the constitutive model and prediction model by comparing with the experiment results. Hu et al. [23] established a 3D FEM, verified the thrust force and torque of the 3D finite element model through experiment and studied the influence of edge radius on chip formation by using the model. Chen et al. [24] established a 2D FEM composed of SiCp/Al6063, explored the influence of particle distribution on the cutting mechanism and concluded that the processability of material with uniform particle distribution was better than that of material with random particle distribution. There are few reports on 3D FEM simulation of UVAD of SiCp/Al6063. For mathematical thrust force prediction model of ultrasonic vibration-assisted manufacturing, the researches mainly focused on UVAM and UVAD. Ni et al. [25] proposed a theoretical model for calculating the tool and work-piece contact rate (TWCR) in UVAM process, and they studied the

influence of processing parameters on TWCR. The results showed that the cutting force components in UVAM are reduced compared with CM. Although the principle of tool action in drilling and milling is basically the same, there are differences in the mechanical distribution of the tool. Table 1 lists some of the currently accepted models of UVAD. Lu et al. [26] proposed an UVAD thrust force prediction model and discussed the influence of amplitude on thrust force adjustment theoretically. Chang et al. [27] proposed a thrust force predicted model during UVAD of 6061-t6 aluminum alloy. The maximum errors were only 7% when using the proposed model. Shi et al. [28] established a mathematical model of average thrust force in the process of UVAD based on the principle of UVAD. Feng et al. [29] formed a soft coefficient response surface by using the experiment data, which described the change rules of soft coefficient visually, and then established a thrust force prediction model. The result showed that the error of the thrust force prediction model is about 10%, and the maximum thrust force error is not more than 23.1%. According to the above research, the errors of the prediction models drilling are different. The maximum error of the proposed prediction model is between 7−23%.

Table 1. The Mathematical thrust force prediction model of UVAD.

Author	Year	Reference	The Mathematical thrust force prediction model of UVAD
Lu et al.	2007	[26]	$F_x = \left(1 + \frac{\cos^{-1}\left(-\frac{vT}{2\pi a}\right)}{2\pi} - H\left(\cos^{-1}\left(-\frac{vT}{2\pi a}\right)\right)\right) \cdot \frac{w\tau a_p \cos(K - G(a))}{\sin(G(a)) \cdot \cos(K - G(a))}$
Chang et al.	2009	[27]	$\Delta P_i = F_{l,T} \sin p \cos \eta_d + F_{l,C} \sin \eta_d + F_{pt}$
Shi et al.	2019	[28]	$F = F_f - \frac{2\pi^2 f^2 A^2 m \sin(2\pi f t_t) \cdot \sin\left(2\pi f t_t + \cos^{-1}\left(\frac{v_0}{2\pi f A}\right)\right)}{v_0\left(\frac{1}{f} - t_t\right)}$
Feng et al.	2019	[29]	$F_Z = F_1 + F = 2\left(\int_{\frac{d'}{2}}^{\frac{d}{2}} \frac{dF_l}{dr} dr + \int_0^{\frac{d'}{2}} \frac{dF_c}{dr} dr\right)$

Although the ultrasonic vibration-assisted machining is applied widely in engineering, some scholars have established the mathematical prediction model and 3D FEM to analyze the thrust force and chip morphology. However, the UVAD mathematical prediction model is not accurate enough for SiCp/Al6063 composite materials, and the FEM is almost absent. Thus, there are a lot of works to research. In this study, the difference between UVAD and CD of the SiCp/AL6063 is studied. A mathematical prediction model considering the ultrasonic vibration-assisted of the work-piece is established to calculate the thrust force of UVAD of SiCp/AL6063. A 3D FEM for the thrust force and chip morphology analysis are subsequently researched based on ABAQUS software. Finally, CD and UVAD of drilling SiCp/Al6063 experiments were performed.

2. Thrust force prediction model of UVAD

In this part, a modified mathematical thrust force prediction model of UVAD is established. The model is mainly based on the following aspects: the CD thrust force prediction model and the motion relationship between UVAD and CD.

2.1. The mathematical thrust force prediction model of CD

For the research on the mathematical thrust force prediction model of CD, the mathematical thrust force model is divided into two parts. The first part is the cutting force on the main cutting edge, which is represented here as F_l. The second part is the cutting force on the chisel edge, which is expressed by F_c. The sum of the two parts is equivalent to the thrust force. The mathematical thrust force model of CD could be expressed by Eq (1).

$$F_f = F_l + F_c \tag{1}$$

In the prediction model, the thrust force of the main cutting edge and the transverse cutting edge are defined by Elhachimi et al. [30], which is expressed by Eqs (2) and (3), respectively.

$$F_l = 2k_{AB}\int_{\frac{d'}{2}}^{\frac{d}{2}} \frac{rv_0(\sin(\lambda_n-\gamma_n-\xi)\sin p-\cos p)\sin p\cos\xi}{2\sin\phi_n\cos(\phi_n+\lambda_n-\gamma_n)(r^2-t^2)^{1/2}}dr \tag{2}$$

Here, r represents the radius length of any point of the main cutting edge, v_0 is the feed rate, and the diameter of the tool is indicated by d, the half-edge angle of the drill tip is p, the dip angle of the cutter's edge is ψ, the lip spacing is $2w$, the chisel edge diameter is d', which are shown in Figure 2.

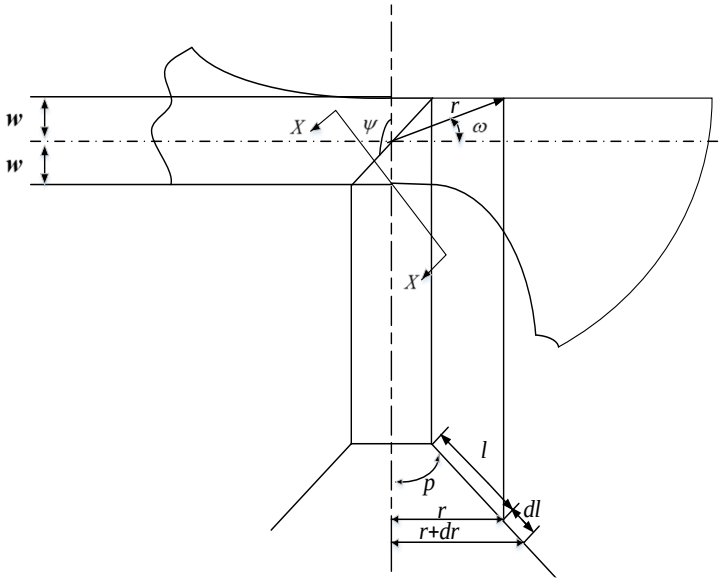

Figure 2. The geometry diagram of the main cutting edge.

Also, ϕ_n is the normal shear Angle, γ_n is the dynamic normal rake Angle, λ_n is the normal friction Angle of the interface between the cutter and chip, i and ξ are the dynamic tool cutting

inclination angle and intermediate angle respectively, which are shown in Figure 3.

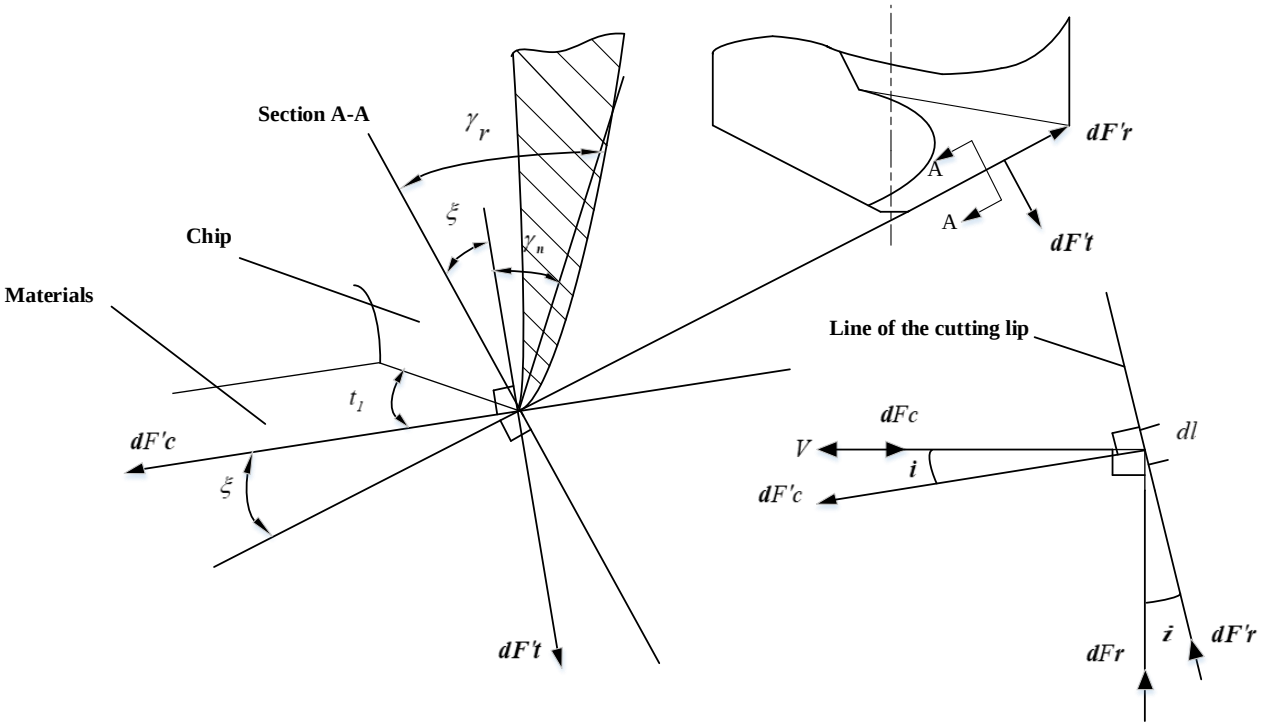

Figure 3. Schematic diagram of cutting force on the main cutting edge.

$$F_c = 2k_{AB}\int_{r_0}^{\frac{d'}{2}} \frac{v_0 \cos\gamma_f \cos(\phi_d-\gamma_d)}{2\sin\phi_d \cos(\phi_d+\lambda_d-\gamma_d)} \cdot \left(\cos\gamma_f - \tan(\phi_d-\gamma_d)\sin\gamma_f\right) dr \tag{3}$$

Where, γ_d is the dynamic angle before cutting, γ_f is the angle between the cutting speed and feed rate, ϕ_d is the dynamic shear angle, and λ_d is the frictional angle between tool and chip. In the process of UVAD, the thrust force near the axial part could be ignored in model [31]. Wiriyacosol et al. [32] concluded that γ_0 could be ignored in drilling small holes, and γ_0 was treated as 0 in this study, and these parameters were determined from the transverse edge model [29].

2.2. The mathematical thrust force prediction model of UVAD

In the process of the UVAD, it could be divided into countless ultrasonic vibration-assisted cycles. Therefore, the thrust force of one cycle in the ultrasonic vibration-assisted motion is obtained, and the total thrust force of the ultrasonic vibration-assisted motion is obtained by integral summation methods. Since the cutting edge of the tool has symmetry, it is generally assumed that the radial forces in the drilling process cancel each other. And its motion form could be regarded as the superposition of the CD motion and the UVAD motion. In the CD, the axial feed rate displacement of the tool is expressed in Eq (4), and the velocity is expressed in Eq (5):

$$y_0(t) = v_0 t \tag{4}$$

$$v_0(t) = y_0'(t) = v_0 \tag{5}$$

The motion of UVAD could be regarded as the vibration motion (Amplitude A, Frequency f) adding on the CD. The motion curves are shown in Figure 4. The axial displacement of the ultrasonic vibration-assisted movement is expressed in Eq (6), and Eq (7) respectively:

$$y_1(t) = A\sin(2\pi ft) \tag{6}$$

$$v_1(t) = y_1'(t) = 2\pi Af\cos(2\pi ft) \tag{7}$$

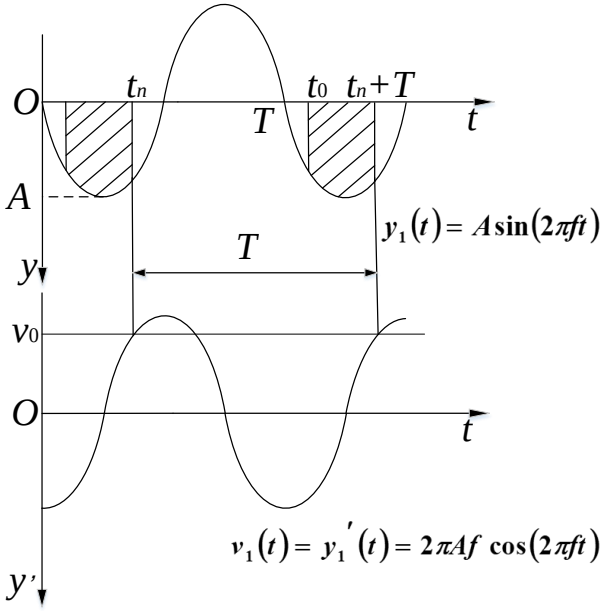

Figure 4. The superimposed amplitude function curve of UVAD.

According to Eqs (4)–(7), the tool displacement in the UVAD is Eq (8), and the velocity could be expressed as Eq (9):

$$y(t) = y_0(t) + y_1(t) = v_0 t + A\sin(2\pi ft) \tag{8}$$

$$v(t) = v_0(t) + v_1(t) = v_0 + 2\pi Af\cos(2\pi ft) \tag{9}$$

Within one cycle time T, when the UVAD feed rate is 0, it could be identified that the tool starts to leave from the work-piece. The Eq (10) can be obtained:

$$t_n = \frac{\cos^{-1}\left(-\frac{v_0}{2\pi Af}\right)}{2\pi f} \tag{10}$$

In air cutting period (t_0-t_n), the displacement of tool was equal to the amplitude function superimposed by ultrasonic vibration, which could be expressed as Eq (11), and the actual drilling time t_t in one cycle of UVAD could be expressed as Eq (12):

$$v_0(t_0 - t_n) = A\sin(2\pi ft_n) - A\sin(2\pi ft_0) \tag{11}$$

$$t_t = (t_n + T) - t_0 = \frac{\pi - \cos^{-1}\left(\frac{v_0}{2\pi Af}\right)}{2\pi f} + \frac{1}{f} - t_0 \tag{12}$$

Supposed that the mass of the tool is m (Tool's mass is about 30 g), Eq (13) is obtained from the kinetic energy theorem:

$$F_0 y = \frac{m\left(v_{t_n+T}{}^2 - v_{t_0}{}^2\right)}{2} \tag{13}$$

The thrust force of the ultrasonic vibration motion within one cycle of Eq (14) is derived according to Eqs (10)−(13):

$$F_0 = -\frac{2\pi^2 f^2 A^2 m \sin(2\pi f t_t) \sin\left(2\pi f t_t + \cos^{-1}\left(\frac{v_0}{2\pi A f}\right)\right)}{v_0\left(\frac{1}{f} - t_t\right)} \tag{14}$$

According to the integral theorem, the total thrust force in the process of the ultrasonic vibration motion could be expressed as Eq (15):

$$F_s = nF_0 = \int_0^n F_0 \, dn = \int_0^{\frac{h}{v(t)\cdot T}} F_0 \, d\left(\frac{h}{v(t)\cdot T}\right) \tag{15}$$

The UVAD is the superposition of the CD and the ultrasonic vibration motion. Therefore, the thrust force model of UVAD is equal to the sum of average impact force of the ultrasonic vibration motion and the mathematical thrust force model of CD. Finally, the mathematical thrust force model of UVAD could be obtained as Eq (16):

$$F = F_f + F_s = 2k_{AB} \int_{\frac{d'}{2}}^{\frac{d}{2}} \frac{r v_0 (\sin(\lambda_n - \gamma_n - \xi) \sin p - \cos p) \sin p \cos \xi}{2 \sin \phi_n \cos(\phi_n + \lambda_n - \gamma_n)(r^2 - t^2)^{1/2}} dr + 2k_{AB} \int_0^{\frac{d'}{2}} \frac{v_0 \cos \gamma_f \cos(\phi_d - \gamma_d)}{2 \sin \phi_d \cos(\phi_d + \lambda_d - \gamma_d)} \cdot$$

$$\left(\cos \gamma_f - \tan(\phi_d - \gamma_d) \sin \gamma_f\right) dr - \int_0^{\frac{hf}{v(t)}} \frac{2\pi^2 f^2 A^2 m \sin(2\pi f t_t) \sin\left(2\pi f t_t + \cos^{-1}\left(\frac{v_0}{2\pi A f}\right)\right)}{v_0\left(\frac{1}{f} - t_t\right)} d\frac{hf}{v(t)} \tag{16}$$

3. 3D FEM of the drilling process

The 3D FEM could do better to simulate the stress distribution and the chip morphology during the process of drilling. In this part, using the ABAQUS/Explicit dynamic solver module, the 3D FEM of UVAD and CD were established. The processing properties of SiCp/AL6063, the stress distribution and chip morphology were predicted.

3.1. 3D FEM description

The 3D FEM of drilling which was done in ABAQUS is presented in Figure 5(a). In the model, a conical concave surface of the work-piece was established in advance to reduce the number of meshes and increase the simulation efficiency. The work-piece was divided into 12 parts as shown in Figure 5(b), and meshed by the neutral axis meshing method as shown in Figure 5(c). The cutting edge was refined with the adaptive meshing method, which could reduce the error. The 3D FEM of drilling assembly is shown in Figure 5(d). In the tool meshing, the minimum mesh size was 0.01 mm, and it was divided into 9477 elements approximately. In the meshing of the work-piece, the

minimum meshed size was 0.008 mm, and about 276,000 meshes were built. In the drilling process, the part of the chisel edge near the axis is in the state of indentation, which has little effect on the axial force and torque and can be neglected in the process of modeling [31]. The rest of the chisel edge may be considered in orthogonal cutting [30].

According to the research of Nan et al. [33], all element nodes on the tool were coupled to a reference point on the tool's central axis to control the boundary conditions of the tool's movement and simulate the drilling process.

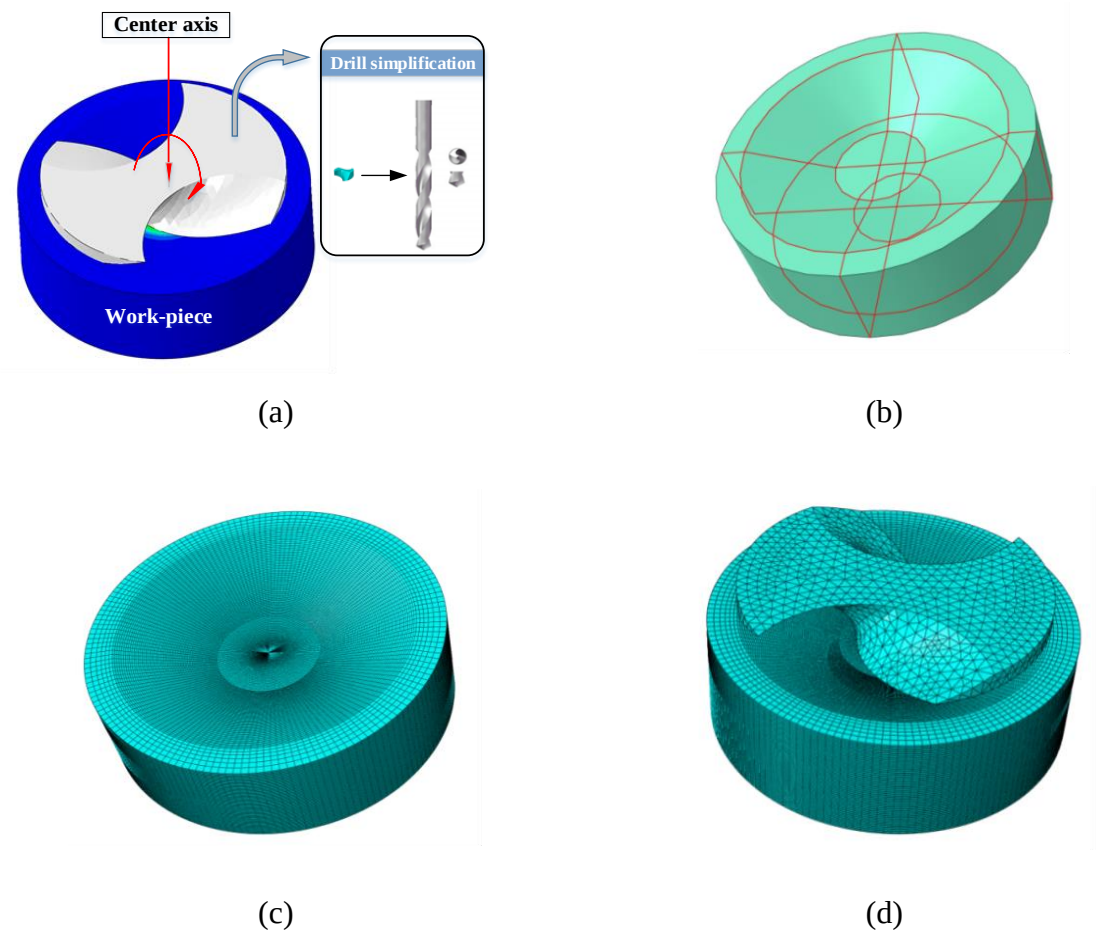

Figure 5. The illustration of 3D FEM. (a) 3D FEM of drilling; (b) Structure division of the work-piece; (c) Meshed diagram of the work-piece; (d) The diagram of drilling assembly.

3.2. Constitutive model and separation criterion for SiCp/Al6063

Constitutive model explains the mechanical behavior of the work-piece and reflects the relationship between stress and strain, strain rate and temperature. In the field of the mechanical cutting simulation, the Johnson-Cook (J-C) model has been used widely. Zhou, Tang et al. [34,35] proposed the J-C equivalent homogenization model for metal matrix composites, and the mechanical parameters of the material are shown in Tables 2 and 3.

Table 2. Mechanical and thermal properties of SiCp/Al6063.

Density (kg/m^3)	Modulus of elasticity (GPa)	Poisson's ratio	Thermal conductivity ($Wm^{-1}K^{-1}$)	Expansion
2790	158	0.25	157	1.2e-5

Table 3. Mechanical and thermal properties of the diamond-coated carbide tool.

Material	Density (kg/m^3)	Modulus of elasticity (GPa)	Poisson's ratio	Thermal conductivity ($Wm^{-1}K^{-1}$)	Expansion
Diamond coating	3	1	0.2	2000	1.1e-6
YG6	15	0.635	0.25	79	5e-6

In the J-C model, the relationship of strain, strain rate and temperature on the flow stress of SiCp/Al6063 composite material is shown in Eq (17):

$$\bar{\sigma} = (A + B[\varepsilon]^n)\left(1 + C\ln\left[\frac{\dot{\varepsilon}}{\dot{\varepsilon_0}}\right]\right)\left(1 - \left[\frac{T - T_{room}}{T_{melt} - T_{room}}\right]^m\right) \tag{17}$$

where $\bar{\sigma}$ is equivalent stress, A is the initial yield strength, B is the hardening modulus, C is the correlation coefficient of strain rate, m is the thermal softening coefficient, n is the index of work hardening, ε is the equivalent plastic strain, $\dot{\varepsilon}$ is plastic strain rate, $\dot{\varepsilon_0}$ is the reference strain rate, T_{room} is the room temperature, T_{melt} is the melting temperature of materials.

The constitutive model parameters were adopted by the reference [22], which were shown in Table 4.

Table 4. J-C constitutive model parameters of SiCp/Al6063.

A(MPa)	*B*(MPa)	*n*	*C*	*m*
446.68	323.39	0.279	0.012	0.877

Chip separation is the key of drilling simulation. Only when the chip separation principle is correctly selected, the changes in temperature, stress and other fields could be output correctly. Based on the J-C yield stress equation, the critical strain fracture criterion was adopted from reference [36], as shown in Eqs (18) and (19):

$$D = \sum \frac{\Delta\varepsilon^p}{\varepsilon^{pf}} \tag{18}$$

$$\varepsilon^{pf} = \left[D_1 + D_2 \exp\left(D_3 \frac{p}{q}\right)\right] \times \left[1 + D_4 \ln\left(\frac{\dot{\varepsilon^{pl}}}{\dot{\varepsilon_0}}\right)\right] \times \left[1 + D_5\left(\frac{T - T_{room}}{T_{melt} - T_{room}}\right)\right] \tag{19}$$

where, $\Delta\varepsilon^p$ represents the increment of the equivalent plastic strain being loaded, p is the hydrostatic pressure, and q represents Mises stress. The damage parameters (D_1~D_5) are constant. Damage evolution occurs when $D = 1$ is set here. ε^{pf} is the current damage strain, and accumulated damage is the function of average stress, strain rate and temperature. The J-C damage parameters D_1~D_5 of SiCp/Al6063 are shown in Table 5.

Table 5. The damage parameters of J-C model for SiCp/Al6063.

D_1	D_2	D_3	D_4	D_5	Reference
0.071	1.248	-1.142	0.147	0.1	[37]

3.3. Drilling simulation analysis and evaluation

The results of the numerical simulation of the SiCp/Al6063 are presented in Figure 6, where Figure 6(a),(b) shows the simulation steps of UVAD and CD respectively. The simulation was carried out with the following cutting conditions: Feed rate was 151.6 mm/min, and the vibration frequency of UVAD was 20 kHz. (a1−a5) and (b1−b5) were the results of the two drilling methods at the times (T = 0.12 s, T = 0.18 s, T = 0.24 s, T = 0.36 s, T = 0.48 s), respectively.

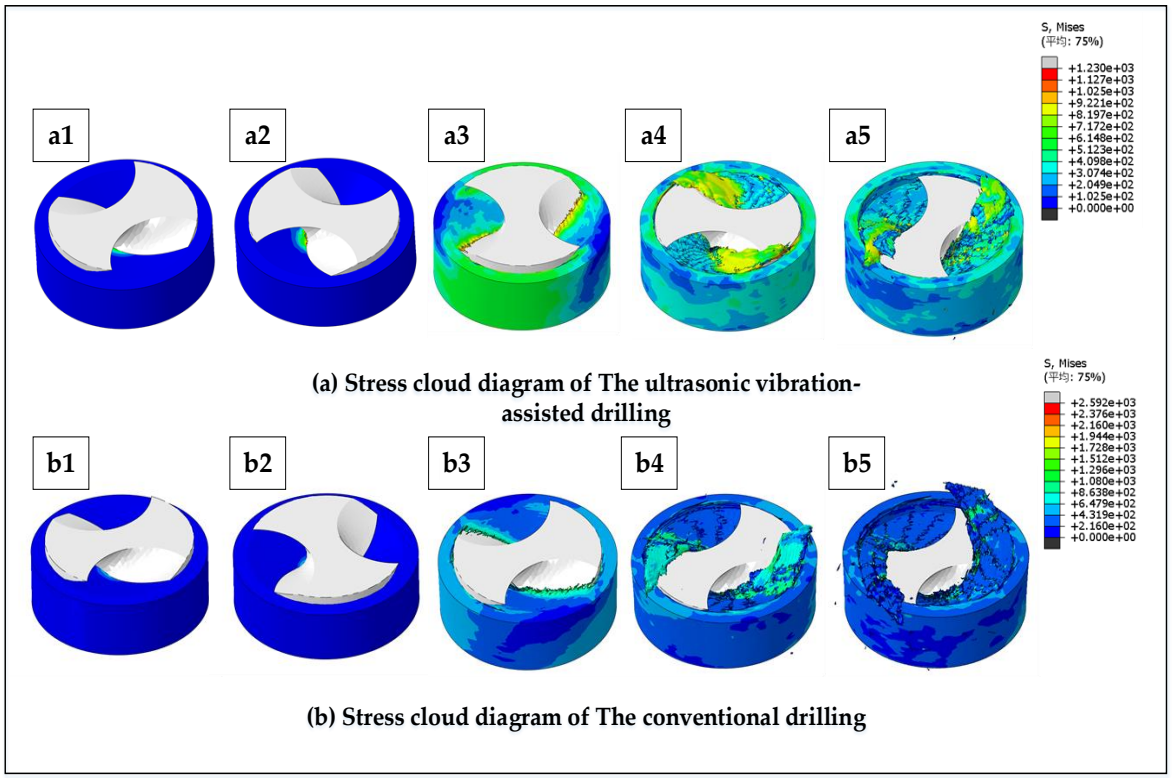

Figure 6. The simulation results of the UVAD and CD (a) Stress diagram of the UVAD; (b) Stress diagram of the CD. (a1−a5) and (b1−b5) represent the states at different times of UVAD and CD FEM, respectively.

The results show that the average Mises stress of UVAD is smaller than that of CD. When the feed rate reaches 151.6 mm/min, the drilling process is relatively stable at the fourth moment. In this moment, the maximum stress of UVAD is 922.1 MPa, and the maximum stress of CD is 1512 MPa. The maximum stress of UVAD reduces by 39.01% compared to CD.

4. Experimental verification

The experiment setup was built and the mathematical prediction model and 3D FEM were verified

with the experiment in this section.

4.1. Scheme of the experiment and design process

The drilling experiment of the SiCp/AL6063 was carried out at Haas VF-3 Vertical Machining Center. The scheme of drilling experiment is shown in Table 6. A diamond-coated carbide tool is used and the tool parameters are shown in Table 7. On the one hand, the work-piece is installed on the dynamometer fixed by the fixture, and the thrust force data signal is collected by the Kistler 9256c2 dynamometer. On the other hand, the signal of the dynamometer will be transmitted to the computer through the 1696A5 eight-channel data transmission line, the Kistler5697A signal acquisition equipment and the Kistler5070 monitoring equipment. In addition, chips of the experiment were collected in groups and observed by scanning electron microscope HITACHI S-3400N. The basic process of experiment is shown in Figure 7.

Table 6. Drilling processing scheme.

Item	Contents
Tool	CVD Diamond coated drill, two teeth
Work-piece material	The 40% volume fraction of SiCp/Al6063 composites
Feed per tooth (mm/rpm)	0.05
Rotation speed (rpm/min)	1516, 2274, 2653, 3032
Fate rate (mm/min)	75.8, 113.7, 132.6, 151.6
Drilling type	CD, UVAD
Ultrasonic vibration frequency (KHZ)	0, 20
Tool	CVD Diamond coated drill, two teeth

Table 7. Tool parameters.

Cutter
Type: single-angle twist drill
Material: diamond-coated bit Dimensions
Diameter 2R = 4.2 mm
Drilling depth h = 8 mm
Web thickness 2w = 0.4 mm
Point angle $2p$ = 118°
Helix angle q = 33°
Chisel edge angle, φ = 130°

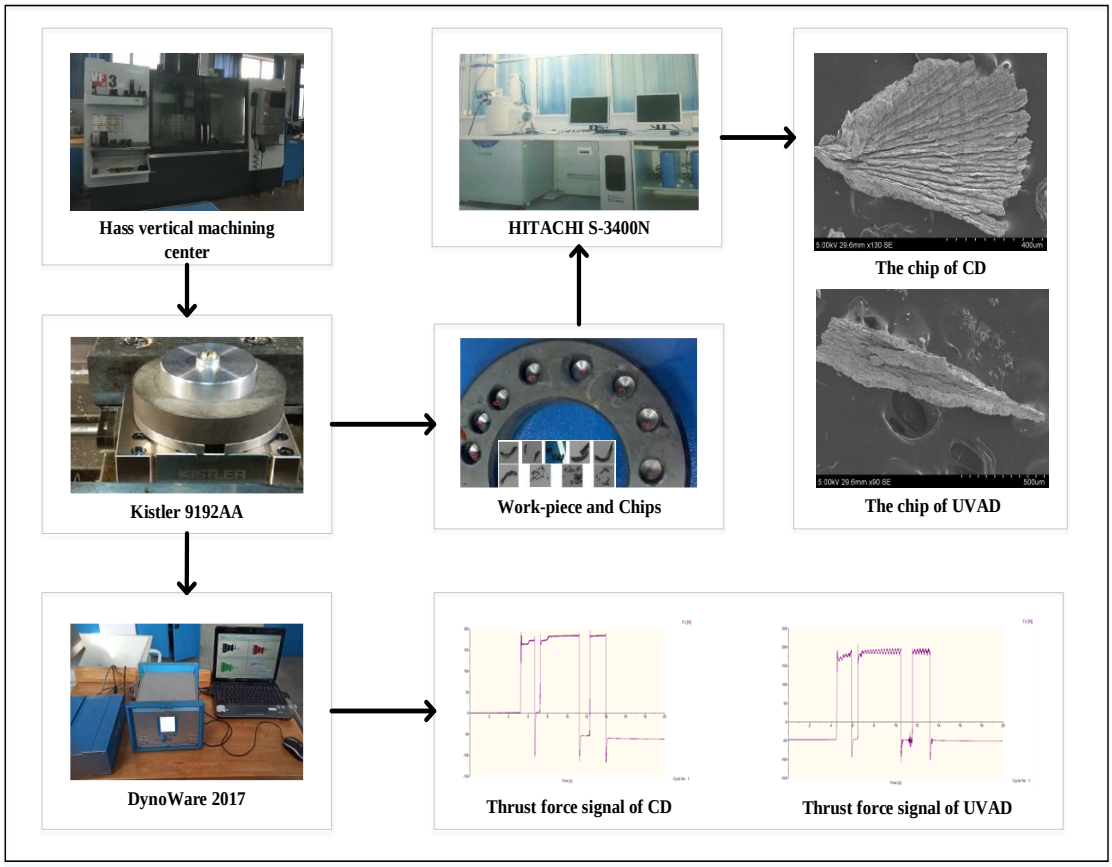

Figure 7. Experimental setup.

4.2. Analysis of the thrust force

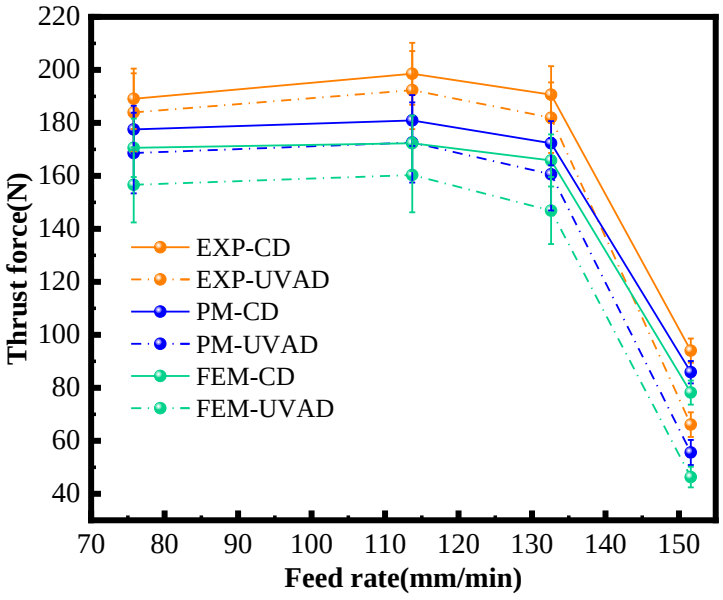

Figure 8. Results of thrust force of the experiment, the 3D FEM and the mathematical thrust force prediction model.

Figure 8 shows the results of the thrust force of the experiment, the 3D FEM and the Mathematical thrust force prediction model. It can be seen that the maximum error between the UVAD mathematical thrust force prediction model and experiment is 12.1%, and the maximum error between the 3D FEM and experiment is controlled in 17.4−26.4%. In the process of UVAD, the modified UVAD mathematical thrust force prediction model and 3D FEM could predict thrust force accurately.

4.3. Analysis of the chip morphology

The chip morphology output of experiment and simulation are shown in Figure 9. The chip shape and size of the simulation were compared with experiment, and the error of the 3D FEM was analyzed.

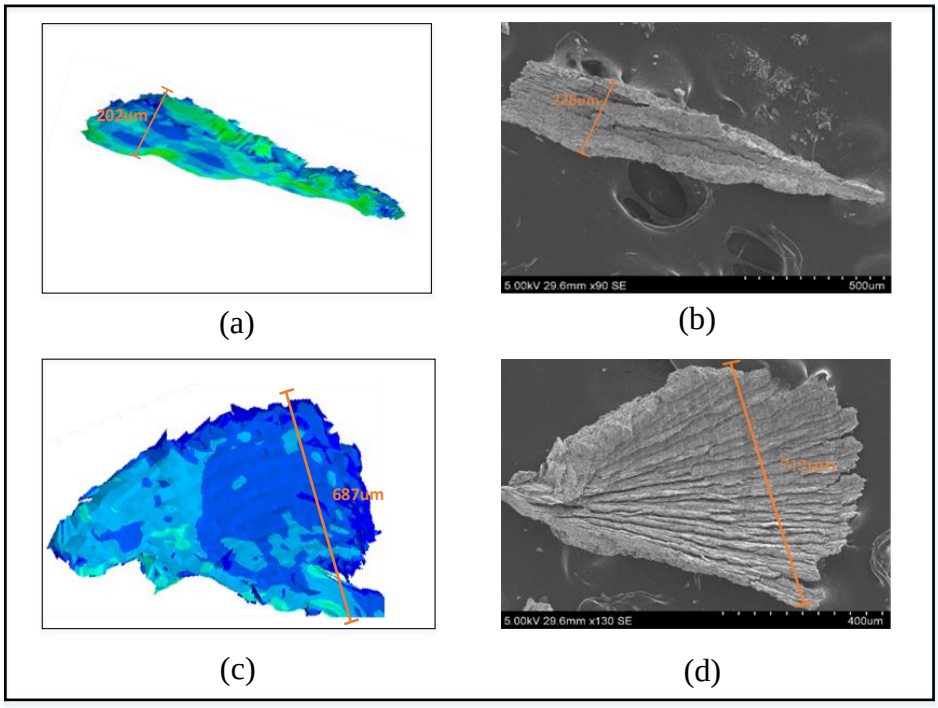

Figure 9. The diagram of the chip morphology. (a) The chip morphology of UVAD in 3D FEM; (b) The chip morphology of UVAD experiment; (c) The chip morphology of CD in 3D FEM; (d) The chip morphology of CD experiment.

In the actual processing, CD produced a wider chip, and the chip bending degree is large. The chip characteristics of UVAD are narrow, and the chip bending degree is small. Compared with CD, UVAD is machined intermittently, which enables the chip morphology change from fan-shaped to aciculiform. The chip width is reduced by 1/3 and evacuated smoothly. The reason for the intermittency is based on the motion relationship of ultrasonic vibration, which has been introduced in detail in Section 2. The intermittent machining mechanism is conducive to damage and remove the chips. The chip morphology obtained in the 3D FEM is similar to the experiment. In the drilling process of the experiment and 3D FEM, the maximum error of chip width is 11.4%. The reason for

the error may be that the chip micro distance in the 3D FEM is measured by the relative displacement of element nodes, while the chip is deformed, but the actual chip distance is measured by the scanning electron microscope directly.

5. Conclusions

In this study, mathematical thrust force prediction model and 3D FE model of drilling SiCp/Al6063 were established to predict the thrust force and chip morphology compared with CD, and drilling experiments for CD and UVAD of SiCp/AL6063 were implemented to validate the validity of the model. The following conclusions are drawn:

1). The experiment results showed that UVAD reduced the thrust force effectively compared with CD. As the feed rate increased, the drilling force decreased more dramatically. When the feed rate reached 151.6 mm/min, compared to CD, UVAD thrust force was reduced by 29.6%, the chip damage efficiency increased by 68.0%. Therefore, UVAD can effectively reduce the thrust force and improve the chip removal efficiency when SiCp/Al6063 material is processed.

2). Compared with the thrust force between mathematical thrust force prediction model and experiment, the maximum error of the thrust force is 12.1%. The results of experiment showed that the thrust force prediction accuracy of the UVAD is relatively high.

3). The 3D FEM of UVAD and CD for SiCp/Al6063 materials were carried out to calculate the thrust force and chip morphology. Compared to the experiment, the deviations of the thrust force and chip width of UVAD are less than 26.4 and 3.5%, and the deviations of the thrust force and chip width of CD are less than 15.4 and 11.4%, respectively. The 3D FEM could simulate the drilling process well.

4). Compared with CD, UVAD is machined intermittently, which enables the chip morphology change from fan-shaped to aciculiform. The chip width is reduced by 1/3 and evacuated smoothly.

Acknowledgments

This research was funded the by Doctoral Research Fund of North China Institute of Aerospace Engineering No. BKY202109 and Graduate Innovation Project funded projects of North China Institute of Aerospace Engineering No. YKY202105.

Conflict of interest

The authors declare there is no conflict of interest.

References

1. Ş. Karabulut, U. Gökmen, H. Çinici, Study on the mechanical and drilling properties of AA7039 composites reinforced with Al2O3/B4C/SiC particles, *Composites, Part B*, **93** (2016), 43−55. https://doi.org/10.1016/j.compositesb.2016.02.054
2. M. A. Kadivar, J. Akbari, R. Yousefi, A. Rahi, M. G. Nick, Investigating the effects of vibration method on ultrasonic-assisted drilling of Al/SiCp metal matrix composites, *Rob. Comput. Integr. Manuf.*, **30** (2013), 344–350. https://doi.org/10.1016/j.rcim.2013.10.001

3. E. Ekici, A. R. Motorcu, Evaluation of drilling Al/SiC composites with cryogenically trea ted HSS drills, *Int. J. Adv. Manuf. Technol.*, **74** (2014), 1495–1505. https://doi.org/10.100 7/s00170-014-6085-z
4. Z. C. Yang, L. D. Zhu, G. X. Zhang, C. B. Ni, B. Lin, Review of ultrasonic vibration-assisted machining in advanced materials, *Int. J. Mach. Tools Manuf.*, **156** (2020), 103594. https://doi.org/10.1016/j.ijmachtools.2020.103594
5. F. D. Ning, W. L. Cong, Ultrasonic vibration-assisted (UV-A) manufacturing processes: State of the art and future perspectives, *J. Manuf. Processes*, **51** (2020), 174−190. https://doi.org/10.1016/j.jmapro.2020.01.028
6. F. D. Ning, W. L. Cong, Z. J. Pei, C. Treadwell, Rotary ultrasonic machining of CFRP: a comparison with grinding, *Ultrasonics*, **66** (2016), 125−132. https://doi.org/10.1016/j.ultras.2015.11.002
7. H. T. Zha, P. F. Feng, J. F. Zhang, D. W. Yu, Z. J. Wu, Material removal mechanism in rotary ultrasonic machining of high-volume fraction SiCp/Al composites, *Int. J. Adv. Manuf. Technol.*, **97 (**2018), 2099−2109. https://doi.org/10.1007/s00170-018-2075-x
8. M. Wang, W. Zheng, M. Zhou, Q. Zhang, Rotary ultrasonic machining of SiCp/Al composites: an experimental study on cutting force and machinability, *Adv. Mech. Eng.*, **11 (**2019), 12. https://doi.org/10.1177/1687814019898329
9. S. Q. Qin, L. D. Zhu, M. Wiercigroch, T. Y. Ren, Y. P. Hao, J. S. Ning, et al., Material removal and surface generation in longitudinal-torsional ultrasonic assisted milling, *Int. J. Mech. Sci.*, **227** (2022), 107375. https://doi.org/10.1016/j.ijmecsci.2022.107375
10. J. Kumabe, T. Soutome, Y. Nishimoto, Ultrasonic super-position vibration cutting of ceramics, *J. Jpn. Soc. Precis. Eng.*, **52** (1986), 1851−1857. https://doi.org/10.2493/jjspe.52.1851
11. X. X. Zhu, W. H. Wang, R. S. Jiang, Z. F. Zhang, B. Huang, X. W. Ma, Research on ultrasonic-assisted drilling in micro-hole machining of the DD6 superalloy, *Adv. Manuf.*, **8** (2020), 405−417. https://doi.org/10.1007/s40436-020-00301-6
12. M. Baraheni, A. B. Bami, A. Alaei, S. Amini, Ultrasonic-assisted friction drilling process of aerospace aluminum alloy (AA7075): FEA and experimental study, *Int. J. Lightweight Mater. Manuf.*, **4** (2021), 315−322. https://doi.org/10.1016/j.ijlmm.2021.03.001
13. X. F. Li, Z. G. Dong, R. K. Kang, Y. D. Wang, J. T. Liu, Y. Zhang, Comparison of thrust force in ultrasonic assisted drilling and conventional drilling of aluminum alloy, *Mater. Sci. Forum*, **861** (2016), 38–43. https://doi.org/10.4028/www.scientific.net/MSF.861.38
14. G. F. Gao, Z. W. Xia, Z. J. Yuan, D. H. Xiang, B. Zhao, Influence of longitudinal-torsional ultrasonic-assisted vibration on micro-hole drilling Ti-6Al-4V, *Chin. J. Aeronaut.*, **34** (2021), 247−260. https://doi.org/10.1016/j.cja.2020.06.012
15. Z. Li, S. M. Yuan, J. Ma, J. Shen, A. D. L. Batako, Cutting force and specific energy for rotary ultrasonic drilling based on kinematics analysis of vibration effectiveness, *Chin. J. Aeronaut.*, **35** (2022), 376−387. https://doi.org/10.1016/j.cja.2020.12.023
16. Y. Li, Y. Yang, Y. Wang, F. Gao, Study on the simulation and experiment of ultrasonic-assisted vibration drilling of Ti6Al4V, in *2022 International Conference on Advances in Modern Physics Sciences and Engineering Technology (ICPSET 2022)*, **2242** (2022). https://doi.org/10.1088/1742-6596/2242/1/012011
17. A. M. Abdelaziz, H. Youssef, M. AI-Makky, H. EI-Hofy, Ultrasonic-assisted drilling of nickel-based super alloy inconel 601: an experimental study, in *19th International Conference on Applied Mechanics and Mechanical Engineering (AMME-19)*, *IOP Conf. Ser.: Mater. Sci. Eng.*, Military Technical College, Egypt, **973** (2020). https://doi.org/10.1088/1757-899X/973/1/012047

18. C. B. Ni, L. D. Zhu, Investigation on machining characteristics of TC4 alloy by simultaneous application of ultrasonic vibration assisted milling (UVAM) and economical-environmental MQL technology, *J. Mater. Process. Technol.*, **278** (2020), 116518. https://doi.org/10.1016/j.jmatprotec.2019.116518
19. Q. L. Niu, L. Jing, C. H. Wang, S. J. Li, X. Y. Qiu, C. P. Li, et al., Study on effect of vibration amplitude on cutting performance of SiCp/Al composites during ultrasonic vibration–assisted milling, *Int. J. Adv. Manuf. Technol.*, **106** (2020), 2219−2225. https://doi.org/10.1007/s00170-019-04796-7
20. Z. Li, D. Y. Zhang, X. G. Jiang, W. Qin, D. X. Geng, Study on rotary ultrasonic-assisted drilling of titanium alloys (Ti6Al4V) using 8-facet drill under no cooling condition, *Int. J. Adv. Manuf. Technol.*, **90** (2017), 3249−3264. https://doi.org/10.1007/s00170-016-9593-1
21. X. X. Xu, Y. L. Mo, C. S. Liu, B. Zhao, Research on drilling experiments of SiC particle reinforced aluminum-matrix composites with ultrasonic vibration, *China. Mech. Eng.*, **21** (2010), 2573. Available from: http://www.cmemo.org.cn/EN/Y2010/V21/I21/2573.
22. T. Dou, H. G. Fu, Z. L. Li, X. Ji, S. S. Bi, Prediction model, simulation, and experimental validation on thrust force and torque in drilling SiCp/Al6063, *Int. J. Adv. Manuf. Technol.*, **103** (2019), 165−175. https://doi.org/10.1007/s00170-019-03366-1
23. F. Hu, L. J. Xie, J. F. Xiang, U. Umer, X. H. Nan, Finite modeling study on small-hole peck drilling of SiCp/Al composites, *Int. J. Adv. Manuf. Technol.*, **96** (2018), 3719−3728. https://doi.org/10.1007/s00170-018-1730-6
24. Y. Chen, X. Zhang, Study on the cutting mechanism of SiCp/Al considering particle size and distribution, *Int. J. Adv. Manuf. Technol.*, **115** (2021), 1211–1225. https://doi.org/10.1007/s00170-021-07225-w
25. C. B. Ni, L. D. Zhu, C. F. Liu, Z. C. Yang, Analytical modeling of tool-workpiece contact rate and experimental study in ultrasonic vibration-assisted milling of Ti–6Al–4V, *Int. J. Mech. Sci.*, **142** (2018), 97−111. https://doi.org/10.1016/j.ijmecsci.2018.04.037
26. Z. S. Lu, L. Yang, Theoretical analysis and simulation of the effect of vibration amplitude on ccutting force in precision ultrasonic vibration cutting, *Key Eng. Mater.*, **329** (2007), 693–698. https://doi.org/10.4028/www.scientific.net/KEM.329.693
27. S. S. F. Chang, G. M. Bone, Thrust force model for vibration-assisted drilling of aluminum 6061-T6, *Int. J. Mach. Tools Manuf.*, **49** (2009), 1070–1076. https://doi.org/10.1016/j.ijmachtools.2009.07.011
28. Y. C. Shi, S. Zong, Z. G. Li, X. L. Yu, Study on the effect of feed rate on the ultrasonic vibration drilling force, *Mach. Tool. Hydraul.*, **47** (2019), 54−56. https://doi.org/10.3969/j.issn.1001-3881.2019.07.012
29. Y. Feng, M. Zhang, Z. H. Zhu, B. H. Jia, X. Y. Wang, Axial cutting force prediction model of titanium matrix composites TiBw/TC4 in ultrasonic vibration–assisted drilling, *Int. J. Adv. Manuf. Technol.*, **105** (2019), 121−135. https://doi.org/10.1007/s00170-019-04149-4
30. M. Elhachimi, S. Torbaty, P. Joyot, Mechanical modelling of high speed drilling. 1: predicting torque and thrust, *Int. J. Mach. Tools Manuf.*, **39** (1999), 553–568. https://doi.org/10.1016/S0890-6955(98)00050-9
31. C. J. Oxford, On the drilling of metals: 1−basic mechanics of the process, *Trans. ASME*, **77** (1955), 103−111. https://doi.org/10.1115/1.4014251
32. S. Wiriyacosol, E. J. A. Armarego, Thrust and torque prediction in drilling from a cutting mechanics approach, *CIRP Ann. - Manuf. Technol.*, **28** (1979), 87−91.

33. X. H. Nan, L. J. Xie, W. X. Zhao, On the application of 3D finite element modeling for small-diameter hole drilling of AISI 1045 steel, *Int. J. Adv. Manuf. Technol.*, **84** (2016), 1927–1939. https://doi.org/10.1007/s00170-015-7782-y
34. L. Zhou, S. T. Huang, D. Wang, X. L. Yu, Finite element and experimental studies of the cutting process of SiCp/Al composites with PCD tools, *Int. J. Adv. Manuf. Technol.*, **52** (2011), 619–626. https://doi.org/10.1007/s00170-010-2776-2
35. L. H. Tang, J. L. Huang, L. M. Xie, Finite element modeling and simulation in dry hard orthogonal cutting AISI D2 tool steel with CBN cutting tool, *Int. J. Adv. Manuf. Technol.*, **53** (2011), 1167–1181. https://doi.org/10.1007/s00170-010-2901-2
36. *Abaqus 6.14 Documentation Abaqus/CAE User's Manual*, 2014.
37. V. K. Doomomra, K. Debnath, I. Singh, Drilling of metal matrix composites: experimental and finite element analysis, *Proc. Inst. Mech. Eng., Part B: J. Eng. Manuf.*, **229** (2015), 886–890. https://doi.org/10.1177/0954405414534227

AIMS Press